A Novel Microwave Attenuator on Multilayered Substrate Integrated Waveguide

Zheng Liu, *Student Member, IEEE*, Lei Zhu, *Fellow, IEEE*, and Gaobiao Xiao, *Member, IEEE*

***Abstract*— In this paper, we propose a novel microwave attenuator based on the multilayered substrate integrated waveguide (SIW). The large loss tangent of Flame Resistant-4 (FR-4) material in the Ku band is employed to design a highly lossy SIW resonator cavity as block element for the exploration of this attenuator. The relative permittivity and loss tangent of FR-4 at high frequency are at first experimentally extracted by testing a fabricated ring resonator on FR-4 substrate. Then the characteristics of single unit of this attenuator versus a few critical geometrical dimensions are studied. Next, an equivalent circuit of this single-unit structure is developed to theoretically predict the propagation characteristics of the designed attenuator in an efficient and effective manner. Finally, an example of SIW-based attenuator is designed and measured. The measured attenuation factor agrees with the simulated and predicted ones in the stopband frequency of our concern. In addition, good impedance matching at input and output ports is satisfactorily realized.**

***Index Terms*— Attenuator, loss tangent, relative permittivity, substrate integrated waveguide (SIW).**

I. Introduction

IN MANY modern communication systems, microwave bandstop filters or attenuators are critical circuit blocks to reject all the unwanted and interference signals or to limit the signal power level. However, most of the reported bandstop filters are reflective ones, and they can hardly achieve good impedance matching at two external ports in the desired stopband. Thus, they may lead to performance degradation of adjacent circuit components [1], [2]. As an effective approach, the attenuators can be employed to circumvent these problems by appropriately equalizing the port impedances with the resonator impedances at resonance in the desired stopband. In this situation, signal power gradually dissipates in a lossy cavity instead of reflection in a bandstop filter. Therefore, the attenuators have been highly demanded in various communication systems.

In general, microwave attenuators can be divided into active and passive structures. Our attenuation herein will be focused on the passive attenuators, since the bias circuits involved in active attenuators may limit their application in some integrated circuits [2]–[5]. Conventional passive attenuators are usually represented by installing a number of lumped resistors in a Π or T topology [6], but they dissipate power over a wide bandwidth and they suffer from poor frequency selectivity in the desired stopband. The amount of attenuation in waveguide attenuators primarily depends on the size and position of the absorbing material placed in a waveguide [7]–[9]. Although a variety of waveguide attenuators can satisfactorily achieve the specified performance, their drawbacks, such as bulky size, heavy weight, and complicated mechanic fabrication, are not suitable for application in microwave integrated circuits. In recent years, the substrate integrated waveguide (SIW) has been widely studied and considered as a promising printed or integrated waveguide due to its compact size, light weight, low cost, and easy integration with other planar circuits [10]–[14]. Very recently, the SIW-based attenuators have been reported in [4] and [10].

In this paper, we propose a novel passive attenuator on the multilayered SIW. The attenuator is composed of an SIW section in shunt connection with seven lossy SIW cavities with different dimensions. Flame Resistant-4 (FR-4) substrate with large loss tangent is applied to constitute and design these lossy cavities for power dissipation. After relative permittivity and loss tangent of FR-4 are experimentally de-embedded with reporting to a fabricated ring resonator, the equivalent circuit of single unit of this attenuator is developed to predict and analyze the performance of the designed attenuator. Finally, a prototype SIW attenuator is designed with our proposed method and the measured results show good performance. Compared with other passive attenuators with lumped resistors or absorptive materials [6]–[10], our proposed attenuator is implemented on two dielectric substrates using the printed circuit board (PCB) fabrication process, and thus it can be easily integrated with other planar integrated circuits.

The remainder of this paper is organized as follows. The relative permittivity and loss tangent of FR-4 are experimentally de-embedded in Section II. Section III demonstrates the effects of a few critical geometrical parameters on the attenuation

Manuscript received July 9, 2015; revised March 1, 2016; accepted May 23, 2016. Date of publication June 29, 2016; date of current version July 14, 2016. This work was supported in part by the Science and Technology Development Fund within the Macao Science and Technology Development Fund under Grant 051/2014/A1, and in part by the Multi-Year Research Grant within the University of Macau, Macau, China, under Grant MYRG2014-00079-FST. Recommended for publication by Associate Editor T.-L. Wu upon evaluation of reviewers' comments.

Z. Liu is with the Key Laboratory of Ministry of Education of Design and Electromagnetic Compatibility of High Speed Electronic Systems, Shanghai Jiao Tong University, Shanghai 200000, China, and also with the Department of Electrical and Computer Engineering, University of Macau, Macau 999078, China (e-mail: lzheng_2012@sjtu.edu.cn).

L. Zhu is with the Department of Electrical and Computer Engineering, Faculty of Science and Technology, University of Macau, Macau 999078, China (e-mail: leizhu@umac.mo).

G. Xiao is with the Key Laboratory of Ministry of Education of Design and Electromagnetic Compatibility of High Speed Electronic Systems, Shanghai Jiao Tong University, Shanghai 200000, China (e-mail: gaobiaoxiao@sjtu.edu.cn).

Color versions of one or more of the figures in this paper are available online at http://ieeexplore.ieee.org.

Digital Object Identifier 10.1109/TCPMT.2016.2572735

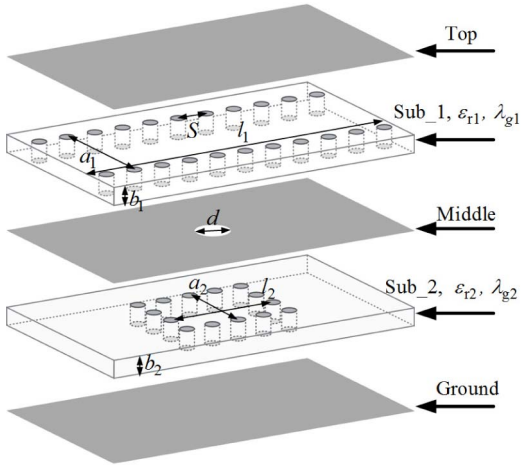

Fig. 1. Schematic of a single unit of the proposed multilayered-SIW attenuator. sub_1 is Taconic TLX with dielectric constant 2.65 and loss tangent 0.0019. sub_2 is FR-4.

characteristics of the single unit of the attenuator. Section IV illustrates and validates the presented equivalent circuit of the single unit structure. An example of the proposed SIW attenuator is designed, fabricated, and measured in Section V. Finally, the conclusion of this paper is given in Section VI.

II. De-Embedding of Lossy Substrate for Attenuator

The schematic of a single unit of the proposed multilayered-SIW attenuator is depicted in Fig. 1. A small circular aperture is etched out in the middle metal surface, and it is used to couple a certain portion of signal power from the upper SIW section to the lower lossy SIW rectangular cavity. Two different substrate materials are Taconic TLX and FR-4 as denoted by Sub_1 and Sub_2 in Fig. 1, for the purpose of signal transmission and dissipation, respectively. The FR-4 is a highly lossy PCB substrate in microwave frequencies, and its dielectric properties need to be accurately known in the concerned frequency range. Otherwise, the inaccurate loss tangent and unstable dielectric constant may seriously degrade the performance of the designed microwave components on this FR-4 substrate [15], [16]. In order to design the lossy SIW resonators on FR-4 in the Ku band, it is our first task to accurately de-embed the relative permittivity and loss tangent of the used FR-4 substrate.

Some approaches to determine the relative permittivity and loss tangent of a substrate material have been presented, such as the single-line method [17], T or ring resonator [18], [19], and bandstop filter method [20]. Following the design procedure given in [19], in this paper, a microstrip ring resonator capacitively coupled with two feeding microstrip lines is designed and fabricated with its fundamental resonant mode operating near 2.0 GHz. The effective dielectric constant of the microstrip line involved in this ring, i.e., $\varepsilon_{\rm re}$, can be obtained as

$$\varepsilon_{\rm re} = \frac{n^2 c}{4\pi^2 r^2 f_n} \tag{1}$$

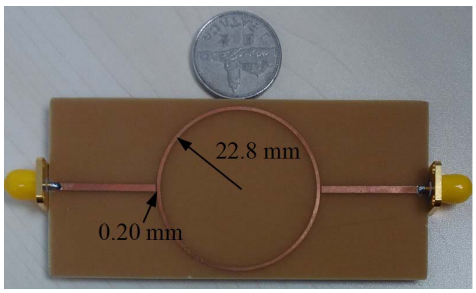

Fig. 2. Fabricated ring resonator with a ring width of 0.5 mm.

where n is the order of the resonant mode ($n = 1, 2, 3 \ldots$) in such a ring resonator, c denotes the light velocity, r is the radius of ring resonator, and f_n is the measured resonant frequency of the nth-order mode.

Using the closed-form formula in [21], the actual relative permittivity, i.e., ε_r, of this substrate can be determined as

$$\varepsilon_r = \frac{(2\varepsilon_{\rm re} - 1)\sqrt{1 + 12h/w} + 1}{\sqrt{1 + 12h/w} + 1} \tag{2}$$

where h is the height of this substrate and w is the strip width of the ring resonator.

Fig. 2 shows the fabricated ring resonator. Due to the weak coupling between the feeding lines and resonator, the unloaded quality factor Q_0 can be approximately determined by its loaded quality factor Q_l under the condition provided in [19] and [21]. The value of Q_l can be calculated by the 3-dB bandwidth of this resonator at resonance. Usually, the unloaded Q_0 of a resonator is primarily attributed by its radiation, conductor, and dielectric losses. For such a ring resonator on the lossy FR-4 substrate at microwave frequency, the dielectric loss occupies a large percentage of the resultant Q_0, and the conductor and radiation losses are not crucial [16]. The value of Q_0 can be reasonably determined by its dielectric loss. Thus, the loss tangent, denoted by $\tan\delta$, of FR-4 can be computed by [21]

$$\tan\delta \approx \frac{1}{Q_0} = \frac{\sqrt{1 - 2 * 10^{-(L_a/10)}}}{Q_l} \tag{3}$$

where L_a denotes the measured insertion loss of this ring resonator.

With the above method, the relative permittivity and loss tangent of the used FR-4 can be experimentally extracted as illustrated in Fig. 3 as a function of frequency. It can be found that the relative permittivity of FR-4 substrate gradually decreases with respect to frequency, while the loss tangent increases. In particular, as the frequency increases from 2.0 to 16.0 GHz, the loss tangent rises by nearly 50%.

III. Operation Multilayered-SIW Attenuator

Fig. 1 depicts the schematic of a single unit of the proposed microwave attenuator formed on a two-layered SIW structure. The main SIW waveguide is formed on the top substrate with small loss tangent, whereas the half-wavelength half-wavelength lossy SIW resonator consist of the lower substrate with high loss tangent. The lossy SIW cavity is connected

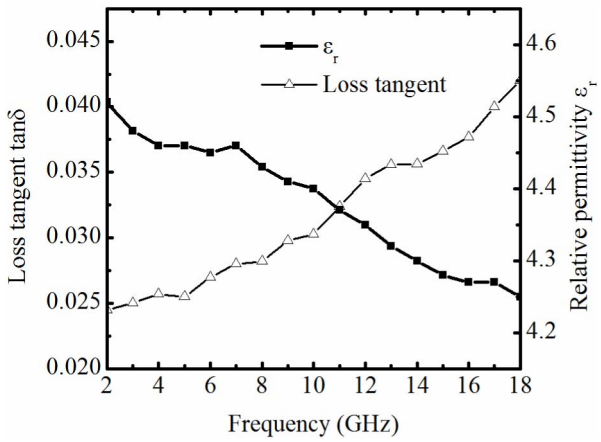

Fig. 3. Experimentally de-embedded relative permittivity and loss tangent of the used FR-4 material with respect to different frequencies.

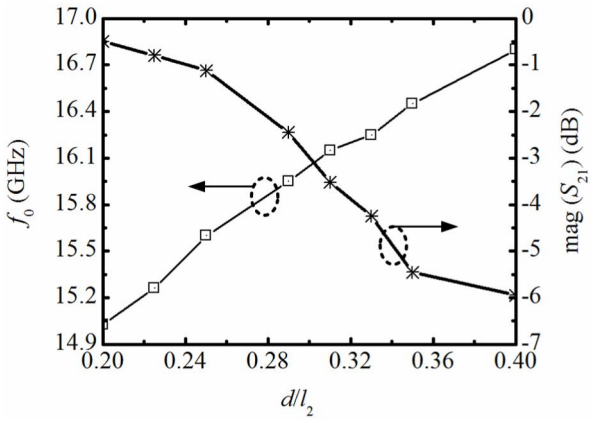

Fig. 4. Attenuation factor and resonant frequency of the single unit of the multilayered SIW attenuator in Fig. 1 versus different values of d/l_2 ($a_1 = 10.3$, $a_2 = 6.6$, $b_1 = b_2 = 1.0$, $l_2 = 10.2$, $S = 2.3$, $\tan\delta = 0.035$, $\varepsilon_{r2} = 4.28$, and via's diameter: 1.2; unit: mm).

in shunt with the SIW waveguide via a circular aperture in the metal surface between them. In order to effectively excite the resonant modes in this unit attenuator, the introduced electric field would better have the strongest magnitude during one period. Meanwhile, it is worthwhile to note that when multicavities are cascaded in the bottom substrate, they cannot be overlapped. Due to the relative permittivity of the TLX material is smaller than that of FR4, λ_{g1} is larger than λ_{g2} for the same dimensions of SIWs. Thus, the length of unit attenuator in the top substrate should be equal to about half a guided wavelength, i.e., $l_1 = 0.5\lambda_{g1}$.

Looking at Fig. 1, we can well understand that the operating frequency band of this single-unit structure mainly depends on the resonant frequency of the lossy SIW resonator and the size of small aperture for coupling. Fig. 4 depicts the resonant frequency and attenuation factor of this simple unit-cell attenuator with respect to the varying diameters of the coupling aperture, where the sizes of the SIW cavity are fixed. As the diameter d of this aperture is enlarged, the operating frequency with minimum S_{21} magnitude gradually moves to higher frequency, and the minimum S_{21} value increasingly falls down.

Now, we would like to apply the perturbation theory to provide insight into the trend of this variation. Assuming that the fundamental mode of the SIW cavity is the TE_{101} mode, the maximum electric field magnitude should be located at the center of this cavity, where the magnetic field magnitude vanishes. As a small aperture exists on the top metal of this SIW cavity shown in Fig. 1, its effect on the lossy SIW cavity can be equivalently considered as a perturbation in electric field. In other words, this cavity is mainly perturbed by a variation in relative permittivity, denoted by $\Delta\varepsilon$, where $\Delta\varepsilon = \varepsilon_{r1} - \varepsilon_{r2}$, $\varepsilon_{r1} < \varepsilon_{r2}$. According to the perturbation theory described in [21], the resonant frequency of the perturbed cavity, denoted by f, can be calculated by

$$\frac{f - f_0}{f_0} \approx -\frac{\int_{s_0} (\Delta\varepsilon \cdot \varepsilon_0 |\vec{E}|^2) ds}{4W} \tag{4}$$

where f_0 is the resonant frequency, W is the stored energy, $|\vec{E}|$ is the electric field in the initial cavity without an aperture,

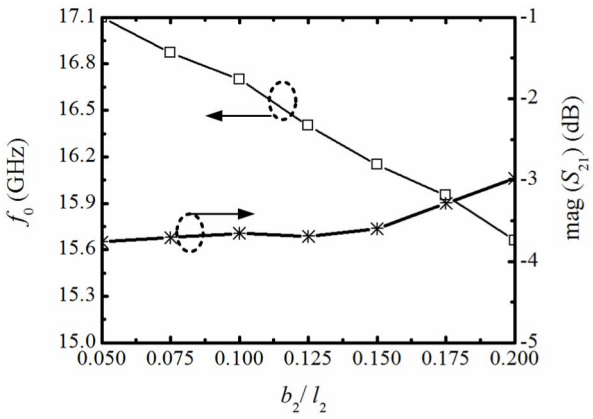

Fig. 5. Attenuation factor and resonant frequency of a multilayered SIW attenuator in Fig. 1 versus different values of b_2/l_2 ($a_1 = 10.3$, $a_2 = 6.6$, $b_1 = 1.0$, $d = 3.1$, $l_2 = 10.2$, $S = 2.3$, $\tan\delta = 0.035$, $\varepsilon_{r2} = 4.28$, and via's diameter: 1.2; unit: mm).

and S_0 is the surface area of the circular aperture, which is a function of the diameter d.

From (4), we can figure out that with increase in d, the resonant frequency of the SIW cavity tends to rise up at the beginning, and the frequency band with high attenuation then moves upward to higher frequency.

Fig. 5 illustrates the attenuation characteristics and resonant frequency of this single-unit attenuator as a function of height or thickness (b_2) in the lower SIW cavity. As b_2 is enlarged, the frequency band with high attenuation is gradually shifted to lower frequency, and its attenuation level is almost unchanged. This variation trend in frequency response can also be explained using the above perturbation theory. In this manner, the circular aperture gradually decreases the total amount of electrical energy stored in the lossy SIW resonator, but hardly gives influence on stored magnetic energy. With the variation of height b_2, the stored magnetic energy varies much more significantly, so the concerned resonant frequency can be expressed as follows relying on magnetic field of the

cavity [21]:

$$\frac{f-f_0}{f_0} \approx -\frac{\int_{V_0}(u_0|\vec{H}|^2)dV}{4W} \tag{5}$$

where V_0 is the varied volume of cavity and it is a function of b_2, and $|\vec{H}|$ is the magnetic field in the resonator.

It is worthwhile to note that the average power handing capacity (APHC) of the SIW is a function of its height. The APHC for the SIW resonator cavity is linearly proportional to its height b_2 [22].

IV. Equivalent Circuit for Analysis and Design

A complete equivalent circuit, inclusive of a small aperture for coupling and lossy SIW cavity, is given and then employed in this section to predict the attenuation characteristics of the proposed attenuator in Fig. 1 through circuit analysis instead of time- and memory-consuming full-wave method. Moreover, the equivalent circuit can provide physical insight into the nature or behavior of the modeled structure.

An electrically small aperture on the broad wall of a rectangular waveguide has been well studied in [23]–[27]. As the outcome of these works, it is well known that the distortion of the field lines in the vicinity of a small aperture primarily depends on the nature of the excitation, and the physical shape and size of the aperture. In other words, the behavior of the aperture is tremendously dependent on the magnetic polarization and electric polarization, responding to the tangential components of magnetic field and the normal components of electric field at the aperture, respectively. These polarizations are functions of the shape and size of the aperture only [26], [27]. Parasitic effects caused by the edge of aperture can be neglected.

Fig. 6(a) depicts the longitudinal view of the multilayered-SIW attenuator in Fig. 1, and the metallic vias are represented by perfect electric conductor for simplicity in analysis. Assume that only the dominant mode in the SIW, TE_{10} mode, is under the situation of propagation, only the three field components, i.e., H_z, E_y, and H_x, are nonzero. The effects of these three field components on the coupling strength of a small aperture can be represented by their equivalent lumped circuit elements in series or shunt connection with two waveguides [26], [27]. Thus, the equivalent circuit of this small aperture can be constituted as illustrated in Fig. 6(b).

In Fig. 6(b), the magnetic field component H_x gives rise to series-inductive coupling, denoted by an inductance L_3, and the magnetic field H_z to shunt-inductive coupling L_2 and L_1, respectively, while the electric field E_y stands for capacitive coupling, denoted by a capacitance C_1. The values of these coupling parameters can be calculated by utilizing a series of design formulas in [27]

$$\frac{Y_1}{Y_2} = \frac{\lambda_{g2}a_{e1}}{\lambda_{g1}a_{e2}} \tag{6}$$

$$\frac{B_{L_2}}{Y_1} = \frac{\left(\frac{\lambda_{g1}}{\lambda_1}\right)^2 \frac{2\pi P}{\lambda_{g1}a_{e1}b_1}\left(1+\frac{a_{e1}}{a_{e2}}\right)}{1-\frac{8\pi P}{\lambda_1^2 b_1}} \tag{7}$$

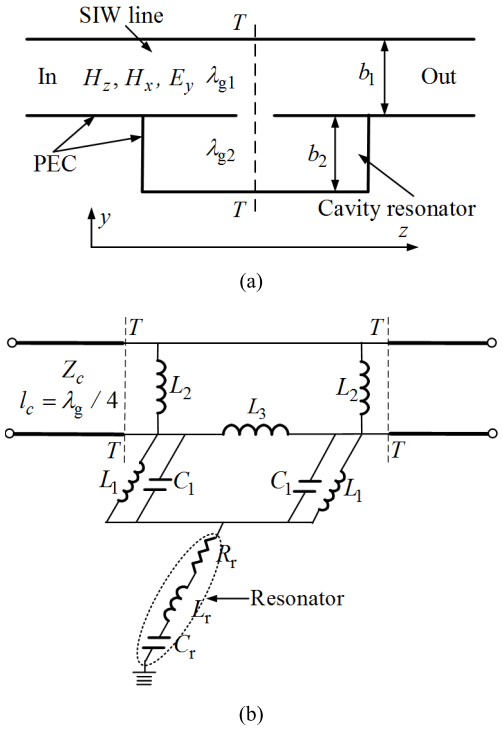

Fig. 6. 2-D view and equivalent circuit of a single unit of the proposed multilayered-SIW attenuator in Fig. 1. (a) Longitudinal view ($b_1 = b_2$). (b) Equivalent circuit.

$$\frac{B_{L_3}}{Y_1} = \left(\frac{\lambda_{g1}}{\lambda_1}\right)^2\left[\frac{1}{M} - \frac{\pi}{a_{e1}^2 b_1}\left(1+\frac{a_{e1}^2}{a_{e2}^2}\right)\right] \tag{8}$$

$$\frac{B_{C_1}}{Y_1} = \frac{B_{L_2}}{Y_1}\frac{a_{e1}}{(a_{e1}+a_{e2})} \tag{9}$$

$$\frac{B_{L_1}}{Y_1} = \frac{B_{L_2}}{Y_1}\frac{a_{e1}}{a_{e2}}. \tag{10}$$

Herein, Y_1 and Y_2 stand for waveguide equivalent impedance, and they can be obtained by the power-voltage definition [21]

$$Y_i = \frac{2a_{\mathrm{ei}}\sqrt{1-(\lambda_i/2a_{\mathrm{ei}})^2}}{\pi b_i \eta_i}, \quad i = 1, 2. \tag{11}$$

where a_{ei} is the equivalent width of SIW [28] and η_i is the wave impedance.

For a centered circular aperture of diameter d, the magnetic and electric polarizations P and M can be obtained by [21]

$$P = \frac{d^3}{12}, \quad M = \frac{d^3}{6}. \tag{12}$$

Meanwhile, the equivalent circuit of a lossy SIW cavity can be represented by a series resonator circuit as illustrated in Fig. 6(b). All the circuit elements involved can be approximately calculated by [21], [28], [29]

$$R_r = \frac{\pi\eta_2}{2Q_0} \tag{13}$$

$$L_r = \frac{\eta_2}{4f} \tag{14}$$

$$C_r = \frac{1}{(2\pi f)^2 L_r}. \tag{15}$$

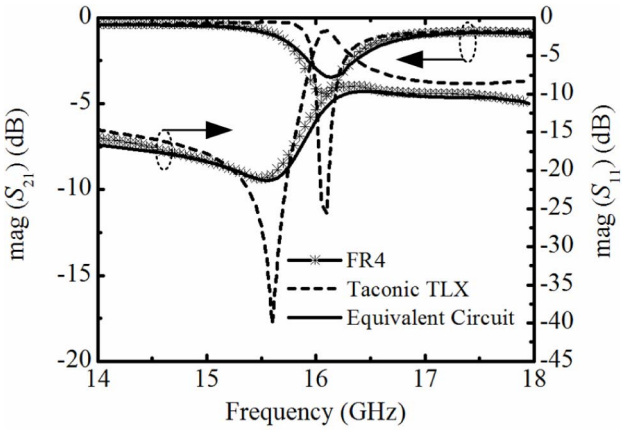

Fig. 7. Comparison among the attenuation factors simulated under different substrate materials and equivalent circuit model. $L_1 = 0.19$ nH. $L_2 = 0.29$ nH. $L_3 = 2.7$ nH. $C_1 = 17$ pF. $R_r = 14\ \Omega$. $C_r = 0.04$ pF. $L_r = 3$ nH. For FR4, $a_2 = 6.6$, $l_2 = 10.2$, and $d = 3.1$. For TLX, $a_2 = 7.55$, $l_2 = 12.35$, and $d = 3.1$ (unit: mm).

Based on (6)–(15), the attenuation characteristics of the single-unit multilayered-SIW attenuator, as shown in Fig. 1, are calculated using the above-described equivalent circuit model. Fig. 7 shows the calculated results compared with those from the full-wave simulation. Although small deviation is observed in Fig. 7, the equivalent circuit still can be applied to approximately but efficiently predict the whole attenuation characteristics of the proposed multilayered-SIW attenuator with complicated geometry. As shown in Fig. 7, good impedance matching at input and output ports can be well gained since the input power dissipates in the lossy cavity. When the resonator cavity is designed using Taconix TLX as substrate, the simulated scattering parameters are also given by comparison. It is clear that the sharp roll-off magnitude response and high attenuation factor are difficult to control and then restrict the freedom of designing an attenuator with wide bandwidth and small attenuation factor.

V. Design Examples and Results

In order to validate our proposed method, an SIW-based attenuator working in the 15.5 GHz with attenuation factor over 10 dB and 10% fractional bandwidth (FBW) is designed. Its geometrical structure is implemented by cascading several half-wavelength lossy resonators with dissimilar dimensions. After the characteristics of single-unit attenuator and its corresponding equivalent circuit model are obtained, the frequency response of the entire attenuator can be estimated using these cascaded equivalent circuit models. Although the obtained results are approximate due to the intrinsic property of all the equivalent circuit methods, the number of required unit attenuators and the initial dimensions of the whole structures can be accurately and efficiently determined by executing our final optimization of its entire layout relying on the commercial EM simulator.

The detailed procedure with our proposed method to design an SIW-based attenuator is summarized as follows.

1) Extract the characteristics of the used FR4 material, i.e., the relative permittivity and loss tangent, with the use of the ring resonator method.

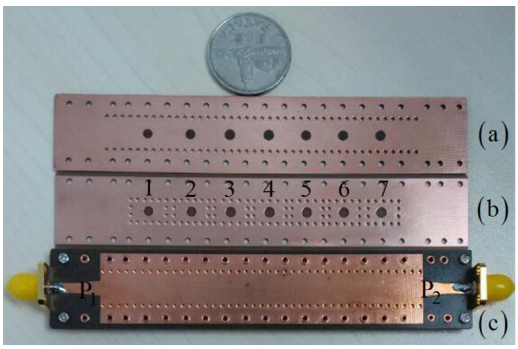

Fig. 8. Fabricated SIW attenuator. (a) Bottom layer of sub_1. (b) Top layer of sub_2. (c) Whole SIW attenuator. $a_1 = 10.3$ and $a_2 = 7$ (unit: mm).

TABLE I
Parameters of Resonator Cavities and Apertures

	d (mm)	l (mm)
1	3.00	10.80
2	3.10	10.50
3	3.25	10.25
4	3.30	9.95
5	3.10	9.60
6	3.00	9.30
7	2.95	9.10

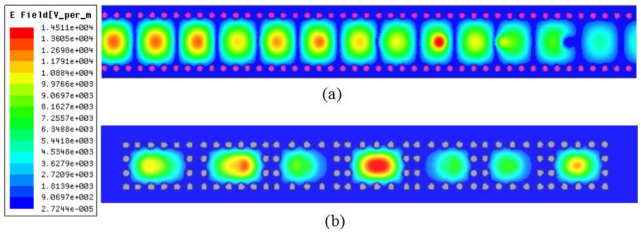

Fig. 9. Electric field distribution of the proposed SIW attenuator at 15.45 GHz (a) on the top metal of the SIW and (b) inside seven lossy resonators.

2) A single-unit attenuator and its corresponding equivalent circuit can be formed up with (6)–(15).
3) Based on the desired attenuation factor and operating bandwidth, the number of unit attenuators can be determined by calculating the frequency responses of equivalent circuit models, and thus the initial dimensions of the whole attenuator can be approximately obtained.
4) The whole structure of the resultant attenuator with multilossy cavities in shunt and transitions at external ports is optimally designed to obtain the satisfactory attenuation performance in a certain stopband.

The conventional tapered microstrip transitions are used to feed this whole attenuator to obtain good impedance matching [30], [31]. The widths/lengths of transitions in P_1 and P_2 ports are found as 4.6/7.2 and 4.55/7.45 mm, respectively.

Fig. 8 depicts the photography of the fabricated multilayered-SIW attenuator, where seven SIW resonators with different dimensions are employed to achieve the desired operating bandwidth and attenuation factor. The distance between two adjacent coupling apertures in sub_1 is set as about $\lambda_{g1}/2$ to effectively excite these resonators and avoid to overlap the position of these resonators. The detailed dimensions of apertures and resonators are listed in Table I.

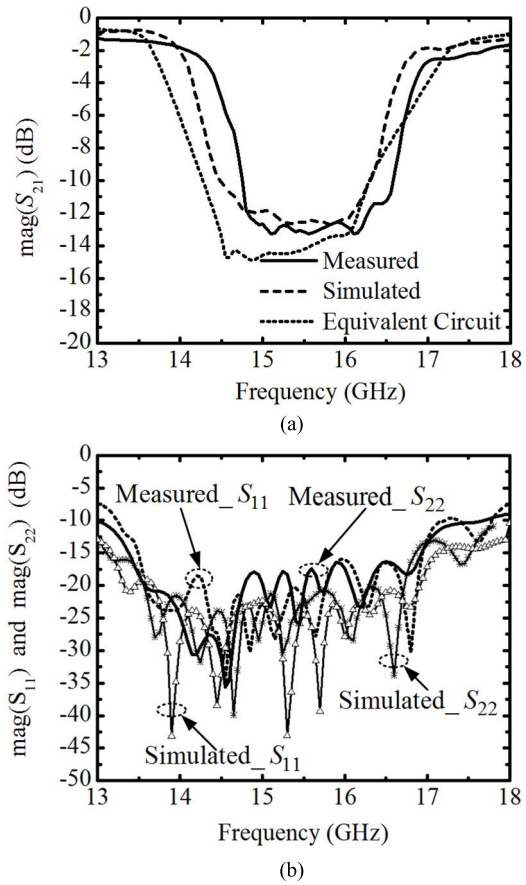

Fig. 10. Comparison among the calculated, simulated, and measured results of the proposed SIW attenuator. (a) Attenuation factors. (b) Return losses.

Fig. 9 depicts the simulated electric field distribution of this designed SIW attenuator. It can be clearly demonstrated that that the input power gradually decays along its propagation direction.

Fig. 10 shows the simulated and measured scattering parameters of the designed multilayered-SIW attenuator. The predicted attenuation factor is given as well by cascading several equivalent circuits as shown in Fig. 6(b). The measured attenuation characteristic is found in reasonably good agreement with the simulated and calculated ones, except that the measured center frequency slightly deviates from the simulated ones by about 2%. This deviation may be caused by the fabricated tolerance and Subminiature version A connecters. However, the fabricated multilayered-SIW attenuator still shows good performance. From Fig. 10(a), we can see that this attenuator has achieved higher than 10-dB attenuation in the frequency range from 14.7 to 16.75 GHz, representing an FBW of about 13%. Moreover, the measured return losses in input and output ports are better than 16 dB in its operating bandwidth as can be observed in Fig. 10(b), so good impedance matching has been achieved as well. Meanwhile, Table II lists the comparison results with other reported results.

For the conventional attenuators, absorbing materials or lumped resistors are always inquired to attenuate the microwave signal. However, our proposed attenuator is simple in geometrical structure since it is fully implemented using the standard PCB fabrication process, so it can be easily integrated with other planar integrated circuits.

TABLE II
COMPARISON WITH OTHER REPORTED MICROWAVE ATTENUATORS

	$\|S_{21}\|$ (dB)	$\|S_{11}\|$ (dB)	FBW (%)	Structure
[2]	-7±0.5	-7	18	Active / Microstrip+Graphene
[4]	-13±0.5	-15	40	Active / HMSIW+PIN diodes
[5]	-4±0.5	-15	62	Passive/ Microstrip+Resistors
[6]	-5±0.5	-20	1～67 GHz	Passive / Resistive π networks
[7]	-2±0.1	/	13	Passive / Rectangular Waveguide+ Loads
[8]	-12.5±0.5	/	14	Passive / Rectangular Waveguide+ absorber
[9]	-14.5±0.5	-15	3	Passive / Rectangular Waveguide+ absorber
[10]	-5±0.5	-15	32	Passive / SIW+ Resisters
This Work	**-12.5±0.5**	**-16**	**13**	**Passive/SIW**

VI. CONCLUSION

In this paper, a multilayered-SIW microwave attenuator is presented by forming a few lossy SIW cavities in shunt connection with the main SIW waveguide. For low cost and easy integration, the FR-4 substrate is used to realize these lossy SIW cavities. This attenuator is realized without needing to install any lumped resistors, bias circuits, or absorptive materials. Compared with the conventional metallic waveguide attenuators, the proposed attenuator is compact in size and easy integration with other planar integrated circuits and SIW circuits. After the single-unit multilayered-SIW attenuator is described, and analyzed, a practical attenuator with seven lossy SIW cavities is designed, fabricated, and measured. The measured results show good performance as expected and are in good agreement with the simulated and predicted ones.

REFERENCES

[1] J.-Y. Shao and Y.-S. Lin, "Millimeter-wave bandstop filter with absorptive stopband," in *Proc. IEEE MTT-S Int. Microw. Symp. (IMS)*, Tampa, FL, USA, Jun. 2014, pp. 1–4.

[2] L. Pierantoni, D. Mencarelli, M. Bozzi, R. Moro, and S. Bellucci, "Graphene-based electronically tunable microstrip attenuator," in *Proc. IEEE MTT-S Int. Microw. Symp. (IMS)*, Tampa, FL, USA, Jun. 2014, pp. 1–3.

[3] J. K. Hunton and A. G. Ryals, "Microwave variable attenuators and modulators using PIN diodes," *IRE Trans. Microw. Theory Techn.*, vol. 10, no. 4, pp. 262–273, Jul. 1962.

[4] R. F. Xu, A. J. Farral, and P. R. Young, "Analysis of loaded substrate integrated waveguides and attenuators," *IEEE Microw. Wireless Compon. Lett.*, vol. 24, no. 1, pp. 62–64, Jan. 2014.

[5] H.-R. Ahn and I. Wolff, "Asymmetric ring-hybrid phase shifters and attenuators," *IEEE Trans. Microw. Theory Techn.*, vol. 50, no. 4, pp. 1146–1155, Apr. 2002.

[6] D. Raicu, "Multiterminal distributed resistors as microwave attenuators," *IEEE Trans. Microw. Theory Techn.*, vol. 42, no. 7, pp. 1140–1148, Jul. 1994.

[7] W. Larson, "Inline waveguide attenuator (correspondence)," *IEEE Trans. Microw. Theory Techn.*, vol. 12, no. 3, pp. 367–368, May 1964.
[8] S. Varsha, N. Y. Joshi, R. K. Atrey, and S. K. Pathak, "Design of X-band waveguide attenuator," in *Proc. Int. Conf. Recent Adv. Microw. Theory Appl. (MICROWAVE)*, Jaipur, India, Nov. 2008, pp. 745–747.
[9] Y. Zhang, "A novel structure of the power equalizer for millimeter wave applications," *Microw. Opt. Technol. Lett.*, vol. 50, no. 10, pp. 2504–2506, Oct. 2008.
[10] D.-S. Eom and H.-Y. Lee, "An X-band substrate integrated waveguide attenuator," *Microw. Opt. Technol. Lett.*, vol. 56, no. 10, pp. 2446–2449, Oct. 2014.
[11] S. W. Wong, K. Wang, Z.-N. Chen, and Q.-X. Chu, "Electric coupling structure of substrate integrated waveguide (SIW) for the application of 140-GHz bandpass filter on LTCC," *IEEE Trans. Compon., Packag., Manuf. Technol.*, vol. 4, no. 2, pp. 316–322, Feb. 2014.
[12] M. L. Coq *et al.*, "Miniaturized C-band SIW filters using high-permittivity ceramic substrates," *IEEE Trans. Compon., Packag., Manuf. Technol.*, vol. 5, no. 5, pp. 620–626, May 2015.
[13] X.-P. Chen and K. Wu, "Self-packaged millimeter-wave substrate integrated waveguide filter with asymmetric frequency response," *IEEE Trans. Compon., Packag., Manuf. Technol.*, vol. 2, no. 5, pp. 775–782, May 2015.
[14] M. Bozzi, A. Georgiadis, and K. Wu, "Review of substrate-integrated waveguide circuits and antennas," *IET Microw., Antennas Propag.*, vol. 5, no. 8, pp. 909–920, Jun. 2011.
[15] V. P. R. Magri, R. A. A. Lima, M. M. Mosso, and C. S. Silva, "Substrate integrated wave guide filter at 10 GHz using commercial FR-4 lossy substrate," in *Proc. IEEE MTT-S Int. IMOC*, Belém, Brazil, Nov. 2009, pp. 595–599.
[16] A. R. Djordjevic, R. M. Biljie, V. D. Likar-Smiljanic, and T. K. Sarkar, "Wideband frequency-domain characterization of FR-4 and time-domain causality," *IEEE Trans. Electromagn. Compat.*, vol. 43, no. 4, pp. 662–667, Nov. 2001.
[17] N. J. Farcich, J. Salonen, and P. M. Asbeck, "Single-length method used to determine the dielectric constant of polydimethylsiloxane," *IEEE Trans. Microw. Theory Techn.*, vol. 56, no. 12, pp. 2963–2971, Dec. 2005.
[18] K.-P. Latti, M. Kettunen, J.-P. Strom, and P. Silventoinen, "A review of microstrip T-resonator method in determining the dielectric properties of printed circuit board materials," *IEEE Trans. Instrum. Meas.*, vol. 56, no. 5, pp. 1845–1850, Oct. 2007.
[19] J.-M. Heinola, K.-P. Latti, P. Silventoinen, J.-P. Strom, and M. Kettunen, "A new method to measure dielectric constant and dissipation factor of printed circuit board laminate material in function of temperature and frequency," in *Proc. IEEE 9th Int. Symp. Adv. Packag. Mater., Process., Properties Interfaces*, Mar. 2004, pp. 235–240.
[20] G. C. Hock, C. K. Chakrabarty, Emilliano, and M. H. Badjian, "Dielectric verification of FR4 substrate using microstrip bandstop resonator and CAE tool," in *Proc. IEEE MICC*, Kuala Lumpur, Malaysia, Dec. 2009, pp. 894–898.
[21] D. M. Pozar, *Microwave Engineering*, 4th ed. New York, NY, USA: Wiley, Nov. 2012.
[22] Y. J. Cheng, K. Wu, and W. Hong, "Power handling capability of substrate integrated waveguide interconnects and related transmission line systems," *IEEE Trans. Adv. Packag.*, vol. 31, no. 4, pp. 900–909, Nov. 2008.
[23] A. Datta, A. M. Rajeek, A. Chakrabarty, and B. N. Das, "S matrix of a broad wall coupler between dissimilar rectangular waveguides," *IEEE Trans. Microw. Theory Techn.*, vol. 43, no. 1, pp. 56–62, Jan. 1995.
[24] A. A. Oliner, "Equivalent circuits for small symmetrical longitudinal apertures and obstacles," *IRE Trans. Microw. Theory Techn.*, vol. 8, no. 1, pp. 72–80, Jan. 1960.
[25] V. M. Pandharipande and B. N. Das, "Coupling of waveguides through large apertures," *IEEE Trans. Microw. Theory Techn.*, vol. 26, no. 3, pp. 209–212, Mar. 1978.
[26] R. Levy, "Analysis and synthesis of waveguide multiaperture directional couplers," *IEEE Trans. Microw. Theory Techn.*, vol. 16, no. 12, pp. 995–1006, Dec. 1968.
[27] N. Marcuvitz, *Waveguide Handbook*. New York, NY, USA: IET, 1951.
[28] F. Xu and K. Wu, "Guided-wave and leakage characteristics of substrate integrated waveguide," *IEEE Trans. Microw. Theory Techn.*, vol. 53, no. 1, pp. 66–73, Jan. 2005.
[29] Y. Huang, "Equivalent circuit of an aperture-coupled lossy cavity," in *Proc. IEEE Antennas Propag. Soc. Int. Symp.*, vol. 2. Jun. 2004, pp. 2043–2046.
[30] D. Deslandes and K. Wu, "Integrated microstrip and rectangular waveguide in planar form," *IEEE Microw. Wireless Compon. Lett.*, vol. 11, no. 2, pp. 68–70, Feb. 2001.
[31] R.-Y. Fang, C.-F. Liu, and C.-L. Wang, "Compact and broadband CB-CPW-to-SIW transition using stepped-impedance resonator with 90°-bent slot," *IEEE Trans. Compon., Packag., Manuf. Technol.*, vol. 3, no. 2, pp. 247–252, Feb. 2013.

Zheng Liu (S'12) was born in Shandong, China, in 1984. He is currently pursuing the Ph.D. degree with Shanghai Jiao Tong University, Shanghai, China.

He was an Exchange Student with the University of Macau, Macau, China, from 2014 to 2015. His current research interests include microwave and millimeter-wave passive and active components and circuits.

Lei Zhu (S'91–M'93–SM'00–F'12) received the B.Eng. and M.Eng. degrees in radio engineering from Southeast University, Nanjing, China, in 1985 and 1988, respectively, and the Ph.D. degree in electronics engineering from the University of Electro-Communications, Tokyo, Japan, in 1993.

He was a Research Engineer with Matsushita-Kotobuki Electronics Industries Ltd., Tokyo, from 1993 to 1996. From 1996 to 2000, he was a Research Fellow with the École Polytechnique de Montréal, Montréal, QC, Canada. From 2000 to 2013, he was an Associate Professor with the School of Electrical and Electronic Engineering, Nanyang Technological University, Singapore. Since 2013, he has been a Full Professor with the Faculty of Science and Technology, University of Macau, Macau, China. Since 2014, he has served as the Head of the Department of Electrical and Computer Engineering with the University of Macau. So far, he has authored or co-authored over 310 papers in international journals and conference proceedings. His papers have been cited more than 3700 times with the H-index of 33 (ISI Web of Science). His current research interests include microwave circuits, guided-wave periodic structures, antennas, and computational electromagnetic techniques.

Dr. Zhu was a recipient of the 1997 Asia-Pacific Microwave Prize Award, the 1996 Silver Award of Excellent Invention from Matsushita-Kotobuki Electronics Industries Ltd., and the 1993 First-Order Achievement Award in Science and Technology from the National Education Committee, China. He was the Associate Editor of the IEEE TRANSACTIONS ON MICROWAVE THEORY AND TECHNIQUES from 2010 to 2013, and the IEEE MICROWAVE AND WIRELESS COMPONENTS LETTERS from 2006 to 2012. He served as a General Chair of the 2008 IEEE MTT-S International Microwave Workshop Series on the Art of Miniaturizing RF and Microwave Passive Components, Chengdu, China, and a Technical Program Committee Co-Chair of the 2009 Asia-Pacific Microwave Conference, Singapore. He served as the member of the IEEE MTT-S Fellow Evaluation Committee from 2013 to 2015, and has been serving as the member of the IEEE AP-S Fellows Committee since 2015.

Gaobiao Xiao (M'02) received the B.S. degree from the National University of Defense Technology, Changsha, China, in 1991, the M.S. degree from the Huazhong University of Science and Technology, Wuhan, China, in 1988, and the Ph.D. degree from Chiba University, Chiba, Japan, in 2002.

He was with Hunan University, Changsha, from 1991 to 1997. Since 2004, he has been a Faculty Member with the Department of Electronic Engineering, Shanghai Jiao Tong University, Shanghai, China. His current research interests include numerical methods in electro-magnetic fields, coupled thermo-electromagnetic analysis, microwave filter designs, fiber-optic filter designs, and inverse scattering problems.